

1 **Role of cellulose nanocrystals on hysteretic**  
2 **sorption and deformation of nanocomposites**

3 Mingyang Chen <sup>1, \*</sup>, Benoit Coasne <sup>2</sup>, Dominique Derome <sup>3</sup> and Jan Carmeliet <sup>1</sup>

4 *1. Chair of Building Physics, ETH Zurich, Switzerland*

5 *2. Univ. Grenoble Alpes, CNRS, LIPhy, France*

6 *3. Department of Civil and Building Engineering, Université de Sherbrooke,*  
7 *Canada*

8 \*Correspondence: minchen@ethz.ch

9 **Abstract:** A molecular model of an all-cellulose nanocomposite, with an amorphous cellulose  
10 matrix reinforced by cellulose nanocrystals, is built to study the role of cellulose nanocrystal (CN)  
11 as a nanofiller in the coupled behavior between sorption and deformation. We find two  
12 competitive mechanisms. The first mechanism is the reinforcing effect through CN-matrix  
13 mechanical interaction, which constrains the sorption-induced swelling of the matrix and results in  
14 a reduction of sorption amount and of hysteresis in both sorption and deformation. The second  
15 mechanism is the CN-water interaction, enhancing water sorption in the matrix at the CN-matrix  
16 interface, increasing the sorption-induced swelling of the matrix, and increasing the resulting  
17 hysteresis in sorption and deformation. The final gain/reduction in sorption, swelling and related  
18 hysteresis depends on which of the two effects prevails. These findings shed light on the tailoring  
19 of cellulose-based composites for applications involving sorption and deformation.

20 **Keywords:** *sorption; deformation; hysteresis; all-cellulose nanocomposite*

21

---

22

## 23 **1. Introduction**

24 Cellulose nanocrystal (CN) exhibits high stiffness and strength, high surface  
25 area and unique morphology (Habibi et al. 2010a; Mariano et al. 2014). These  
26 features, together with their great sustainability and biodegradability, make CN  
27 ideal candidate to improve the mechanical properties of various materials (Habibi  
28 et al. 2010b; Mariano et al. 2014; Blanco et al. 2018). In nature, CN serves as  
29 mechanical reinforcement in several biomaterials (Brown 1996, 2004; Anfara et  
30 al. 2002; Williamson et al. 2002). For instance, the stiffness and strength of wood  
31 cell wall mainly come from the reinforcing effect of the microfibrils composed of  
32 CN (Salmén 2004; Derome et al. 2012; Chen et al. 2019b) For man-made  
33 materials, CN is incorporated as reinforcement into a wide range of polymer  
34 matrices such as poly(caprolactone) (Habibi et al. 2008), poly(oxyethylene) (Azizi  
35 Samir et al. 2004) and starch-based polymers (Anglès and Dufresne 2001). It is  
36 also incorporated into cellulosic matrix to form the so-called all-cellulose  
37 composites (ACC) (Qi et al. 2009). Given the chemical homogeneity of ACC, the  
38 reinforcement–matrix interface forms strong bonding. In addition, ACC can be  
39 straightforwardly recycled as the reinforcement and matrix do not require  
40 separation. These advantages make ACC a promising biodegradable “green”  
41 composite (Nishino et al. 2004; Huber et al. 2012).

42 Cellulose being hydrophilic, the responses of CN-reinforced composites to  
43 moisture must be clearly understood and described. The interaction between  
44 composites and moisture is used as an asset for example in CN-reinforced  
45 composites developed for water purification (Yu et al. 2013; Karim et al. 2014;  
46 Liu et al. 2017; Rafieian et al. 2019). Biomaterials such as wood or man-made  
47 composites are in service commonly exposed to environmental moisture

48 conditions, leading to a change of hygromechanical behavior, eventually to  
49 degradation (Patera et al. 2016; Kafy et al. 2016). The amorphous polymeric  
50 matrix of composites has an open microstructure and water can be adsorbed into  
51 the matrix (Kulasinski et al. 2017). During sorption, water creates its own space  
52 by increasing the host porosity. In so doing, water sorption is accompanied by  
53 swelling which results in an intrinsic coupling between sorption and deformation,  
54 commonly referred to as sorption-induced deformation (Barkas 1939; Kulasinski  
55 et al. 2016; Chen et al. 2018, 2020) Further, sorption in nanoporous polymers  
56 displays a strong hysteresis in terms of moisture content versus relative humidity  
57 (RH), but hysteresis collapses in terms of moisture content versus strain (Patera et  
58 al. 2013; Chen et al. 2018). Also seen is a hysteresis in mechanical property  
59 versus moisture content, but not versus hydrogen bonds between polymeric chains  
60 (Chen et al. 2018). The presence of CN makes the coupling between hysteretic  
61 sorption and swelling even more complex as these nanocrystals may play multiple  
62 roles in the coupling physics. CN can influence water sorption: infrared  
63 spectroscopy shows that water molecules form clusters at the CN/matrix interface  
64 (Maréchal and Chanzy 2000; Hofstetter et al. 2006), indicating that the presence  
65 of CN yields hydrophilic interfaces within the composites. In addition, CN can  
66 have mechanical impact on the matrix. The effect of CN as a mechanical  
67 reinforcement has been extensively studied experimentally for different composite  
68 systems (Favier et al. 1995; Taylor 2002). These studies show that CN can  
69 improve the matrix both in terms of stiffness and strength and the improvement  
70 relies on a strongly bonded CN/matrix interface. The multiple roles played by CN  
71 can be competing. For instance, it has been observed experimentally that water  
72 uptake in CN-reinforced nanocomposites decreases monotonically with increasing  
73 CN content (Anglès and Dufresne 2000; de Mesquita et al. 2012; Mariano et al.

74 2014), while some other experiments show that this dependence is non-monotonic  
75 (Sanchez-Garcia and Lagaron 2010; Sánchez-García et al. 2010; Mariano et al.  
76 2014). This suggests that CN enhance sorption in some circumstances while  
77 hinder sorption in others. Moreover, sorption and swelling of CN-based  
78 composites are found to be dependent on moisture history (Derome et al. 2011;  
79 Safari and van de Ven 2016), i.e., hysteresis is present in the sorption and strain  
80 isotherms. For a better understanding of the dependence of composite properties  
81 on CN, the effects of CN on coupling of sorption and deformation and the related  
82 hysteresis have to be clarified.

83 Water sorption in nanocomposites can be modeled by molecular simulations,  
84 including molecular dynamics (MD) and Monte Carlo (MC) simulations (Charlier  
85 and Mazeau 2012; Mazeau and Charlier 2012; Kulasinski et al. 2017; Zhang et al.  
86 2020a, b) Molecular simulations enable exploring the coupling mechanism of  
87 sorption and deformation at the molecular level. Kulasinski and colleagues built a  
88 molecular model of the secondary layer of wood cell wall, which is a bio-  
89 nanocomposite with CN reinforcing the soft amorphous matrix (Kulasinski et al.  
90 2017). The molecular simulation could capture the anisotropy of the mechanical  
91 properties due to the presence of CN. Moisture content is found to be higher in the  
92 composite compared to the matrix and water molecules are found to cluster at the  
93 interface. This phenomenon was confirmed by Charlier and Mazeau, in a slightly  
94 different system which showed that the water molecules mainly remain in the  
95 volume adjacent to the interface (Charlier and Mazeau 2012). Despite these  
96 previous works, a better understanding of the impact of the presence of CN on the  
97 coupled behavior between the sorption and deformation of nanocomposites is  
98 required. Specifically, we will aim in the present paper at elucidating how CN  
99 influences the sorption-induced swelling of the composites and what role CN

100 plays in sorption and deformation hysteresis. To answer these questions, a  
101 molecular model of CN-reinforced cellulose composite, i.e., ACC (all-cellulose  
102 composite), is built to study the role of CN in the coupling between sorption and  
103 deformation of nanocomposites. The influence of CN on mechanical properties is  
104 first clarified, followed by a detailed study on the role of CN in sorption and  
105 sorption-induced deformation of the composite. Finally, the effect of the presence  
106 of CN on sorption and deformation hysteresis is also discussed.

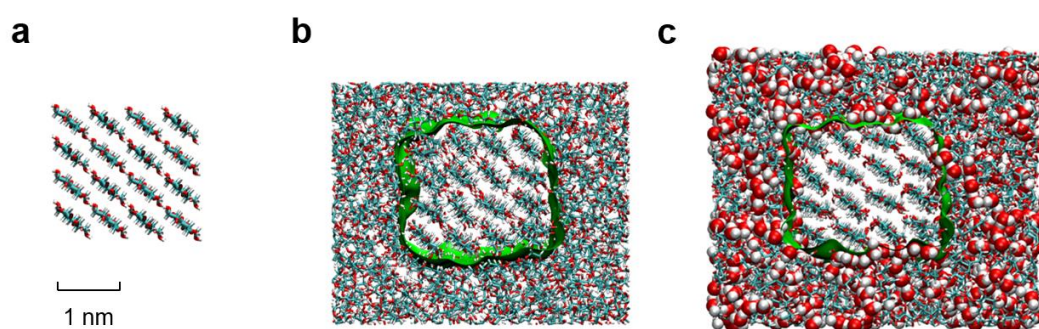
## 107 **2. Models and Methods**

### 108 **2.1. Molecular models**

109 In this paper, we model a cellulose nanocrystal (CN) with 16 polymer chains,  
110 which corresponds to a crystal width about 2 nm. This is consistent with the  
111 experimental observations that CN is generally 2–20 nm wide (Habibi et al. 2010b).  
112 The 16 polymer chains are assembled to make an I $\beta$  CN with the help of Cellulose-  
113 Builder (Figure 1(a)) (Gomes and Skaf 2012). **Based on the atomic-resolution**  
114 **synchrotron and neutron diffraction data reported by Nishiyama et al (Nishiyama et**  
115 **al. 2002, 2003; Wada et al. 2004),** Cellulose-Builder can generate Cartesian  
116 coordinates for all atoms of the specified structure in the Protein Data Bank format,  
117 suitable as starting configurations in molecular dynamics simulations and other  
118 calculations. Then the CN is imported into Material Studio 8.0 and positioned at the  
119 center of an orthogonal box. The remainder of the box volume is packed with  
120 amorphous cellulose (AC), which serves as the matrix of the composite. The  
121 resulting computational domain is used with periodic boundary conditions in all  
122 three directions in order to avoid finite size effect. For practical reason, the CN  
123 extends across the boundaries in the longitudinal direction (Kulasinski et al. 2017).  
124 In other words, CN is infinitely long with an infinitely large degree of

125 polymerization. This generally corresponds to a higher stiffness in the longitudinal  
126 direction compared to composites with finite sized reinforcements. In contrast, the  
127 degree of polymerization of AC is set to 20 cellulose monomers. It has been  
128 verified in our previous work that AC with this 20 cellulose monomers can  
129 reproduce the water sorption isotherms and mechanical properties measured on bulk  
130 AC (Chen et al. 2018). After the packing process, the raw configuration of the  
131 composite is subjected to a series of relaxation processes with the help of MD to  
132 obtain a well equilibrated stress-free configuration. Specifically, the composite is  
133 first relaxed in the *NVT* ensemble, which corresponds to a macroscopic system with  
134 constraints of constant number of particles ( $N$ ), constant volume ( $V$ ) and constant  
135 temperature ( $T$ ), for 2 ns at a temperature  $T = 300$  K. Then the composite is further  
136 relaxed in the *NPT* ensemble with constant number of particles, constant pressure  $P$   
137  $= 0$  and constant temperature  $T = 300$  K for 2 ns. To remove the possible residual  
138 stress generated in the packing process, the temperature is raised to 500 K and  
139 further relaxation is carried out in the *NPT* ensemble for 2 ns with  $P = 1$  MPa to  
140 facilitate the matrix embracing the CN and also to increase the AC density. The CN  
141 is kept rigid at 500 K to prevent its amorphization. Then the external pressure is  
142 removed, and the temperature is reduced back to 300 K. As last step, the composite  
143 is relaxed in the *NPT* ensemble for 4 ns with pressure  $P = 0$  and temperature  $T =$   
144 300 K. The final configuration of the composite after the relaxation process is  
145 shown in Figure 1(b). The volume fraction of CN is found to be 0.27 and the mass  
146 fraction 0.31. The density of AC is  $1.35 \text{ g.cm}^{-3}$  and the density of the CN is  $1.64$   
147  $\text{g.cm}^{-3}$ . Both densities are comparable to experimental results of  $1.48 \text{ g.cm}^{-3}$  (Chen  
148 et al. 2004) and  $1.66 \text{ g.cm}^{-3}$  (Kulasinski et al. 2014) respectively. In dry state, the  
149 dimensions of the computational model are  $5.4 \times 4.4 \times 4.2 \text{ nm}^3$ . For water, we use  
150 the SPC/E water model. The interactions between atoms are modeled by PCFF

151 (Polymer Consistent Force Field) force field (Sun et al. 1994). Practically, the  
152 parameters of PCFF for different elements are directly imported from Material  
153 Studio 8.0. In our previous paper (Chen et al. 2018), we have showed the validity  
154 of combining PCFF and SPC/E in simulating water sorption in amorphous  
155 cellulose by comparing with the experimental sorption isotherms. With PCFF for  
156 amorphous cellulose and SPC/E for water, the simulation captured a lot of  
157 important features such as isotherm shape and sorption hysteresis. In this paper,  
158 we include a cellulose nanocrystal into the amorphous cellulose matrix, but the  
159 chemical composition is kept the same with amorphous cellulose. Thus, we  
160 continue to use the same force field parameters from our previous work (Chen et  
161 al. 2018).



162

163 **Figure 1.** (a) Initial configuration of I $\beta$  CN. (b) Configuration of the composite after relaxation  
164 process. The green surface is the surface of CN determined by Van der Waals radius. (c)  
165 Configuration of the composite with water molecules adsorbed into the matrix.

166 To characterize the role played by the CN in the hygromechanical behavior of  
167 the composite, three systems are built as schematically represented in Figure 2.

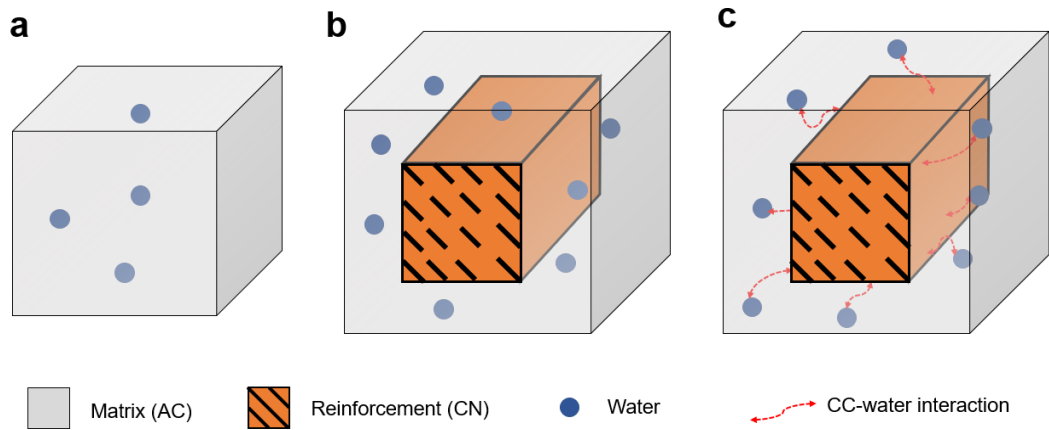
- 168 1. A bulk AC without CN. This system is used to characterize the sorption-  
169 deformation coupling in the pure AC matrix and serves as the reference  
170 when studying the role of CN.
- 171 2. A composite system with a CN in which the interaction between the CN and  
172 water is turned off. Technically, this can be achieved by turning off the  
173 electrostatic and Van der Waals interaction between CN and water. Note

174 that to prevent unphysical water diffusion into CN, the repulsive force  
175 between water and cellulose at very close distances (~0.2 nm in our case) is  
176 maintained on purpose. This means no preferential clustering of water  
177 molecules at the CN/matrix interface will occur, and only a mechanical  
178 reinforcing mechanism of CN is present. This system is termed as *partial-*  
179 *interaction* model as the direct impact of the CN on sorption is on purpose  
180 removed and only the CN-AC interaction is at play. By comparing results  
181 from the bulk AC and the *partial-interaction* model, the mechanical  
182 reinforcing role played by CN through CN-AC interactions can be  
183 characterized.

184 3. A composite with both CN-AC and CN-water interactions included. This  
185 system is termed as *full-interaction* model. In this last model, the presence  
186 of CN affects both AC and water clustering in the interface. Here the role of  
187 CN is not limited to mechanical reinforcement. Since CN shows hydrophilic  
188 surfaces, as there are plenty of hydroxyl groups exposed at its surfaces, the  
189 presence of CN in the composite has a direct impact on water sorption  
190 through the CN-water interaction. This effect can be examined by  
191 comparing the results of *partial-interaction* and *full-interaction* composites.

192 By investigating the behavior of these three systems, we characterize the role of CN  
193 with regard to sorption and mechanics respectively and the coupling between the  
194 two aspects.





195

196 **Figure 2.** Three molecular models considered in this work: **(a)** bulk AC model without  
 197 reinforcement of CN; **(b)** *partial-interaction* composite model with CN-water interactions turned  
 198 off. **(c)** *full-interaction* composite model with CN-water interactions turned on.

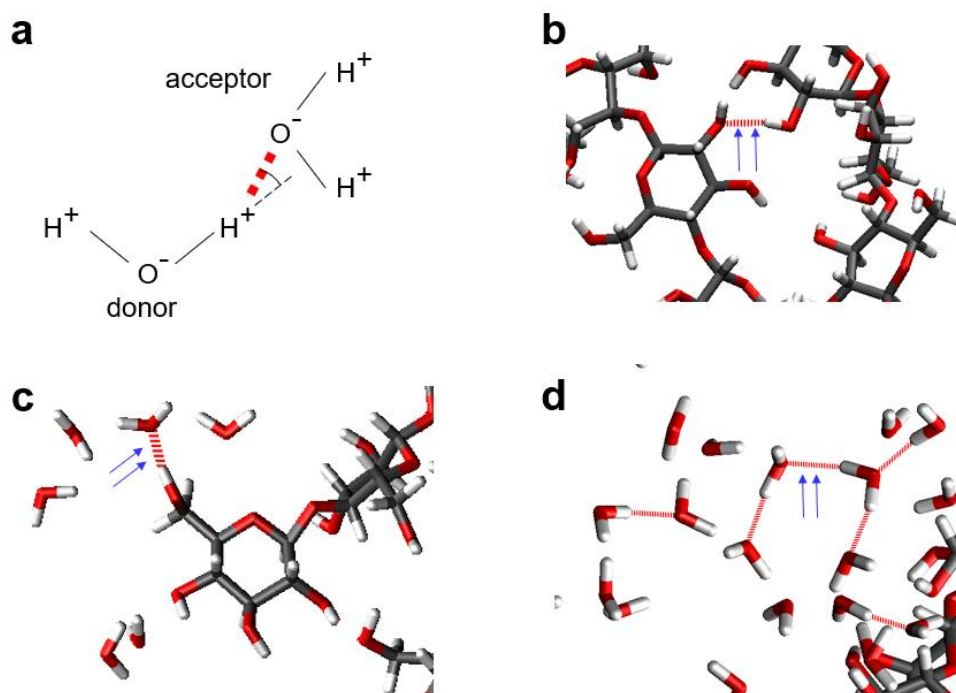
## 199 2.2. Hybrid GCMC/MD simulation

200 To study the coupled effect between sorption and swelling, both aspects are  
 201 modeled based on the osmotic ensemble ( $\mu\sigma T$ ) which allows considering systems at  
 202 constant temperature  $T$ , chemical potential  $\mu$ , and stress  $\sigma$ . This ensemble permits to  
 203 investigate water sorption while allowing for the deformation, or sorption-induced  
 204 deformation (as well as moisture history and thus hysteresis). We perform  
 205 simulations in this osmotic ensemble using a hybrid strategy that combines Grand  
 206 Canonical Monte Carlo (GCMC) simulations with Isobaric-Isothermal MD  
 207 simulations. One can refer to (Chen et al. 2018, 2019a) for a more detailed  
 208 description of this hybrid technique. Specifically, at each chemical potential of  
 209 interest, the free swelling of the composite is simulated using the hybrid  
 210 GCMC/MD molecular simulations with  $\sigma = 0$  and  $T = 300\text{K}$ . Each iteration consists  
 211 of 2000 insertion/deletion MC attempts and 200 MD timesteps. The chemical  
 212 potential is related to relative humidity RH according to  $\mu - \mu_0 = k_B T \ln(RH)$ ,  
 213 where  $\mu_0$  and  $k_B$  are chemical potential of water at saturation and Boltzmann  
 214 constant. Adsorption and desorption are considered by varying the RH from 0 to 1.0  
 215 and from 1.0 back to 0 respectively. A snapshot of the configuration at saturation

216 (RH = 1.0) is displayed in Figure 1(c). It shows that water molecules are only  
217 adsorbed within the matrix - thus outside the CN - and that the composite undergoes  
218 significant swelling.

### 219 **2.3. Characterization of hydrogen bonds**

220 Cellulose is a non-crosslinked polymer so that hydrogen bonds are expected to play  
221 a crucial role in its cohesion and mechanical behavior. As shown in Figure 3 (a), a  
222 hydrogen bond is defined as a physical bond between an O and H atoms separated  
223 by a distance shorter than 0.35 nm and with an angle between the hydrogen donor  
224 and the acceptor smaller than  $30^\circ$ . There are three types of hydrogen bonds as  
225 shown in Figure 3 (b, c, d): bonds formed between cellulose groups and other  
226 cellulose groups ( $\text{HB}^{\text{PP}}$ ), bonds formed between water and cellulose groups ( $\text{HB}^{\text{PW}}$ )  
227 and bonds formed between water molecules and other water molecules ( $\text{HB}^{\text{WW}}$ ).  
228 Specifically,  $\text{HB}^{\text{PP}}$  governs the inter-chain interaction and is thus crucial for the  
229 physical properties of cellulose.  $\text{HB}^{\text{PW}}$  indicates the interaction between cellulose  
230 chain and water molecules, i.e., the adsorbent-adsorbate interaction, thus can be  
231 utilized to identify water-molecules attached to the cellulose chains.  $\text{HB}^{\text{WW}}$  happens  
232 when RH is relatively high and a considerable number of water molecules has been  
233 adsorbed. In this paper, we mainly focus on polymer-related hydrogen bonds, i.e.,  
234  $\text{HB}^{\text{PP}}$  and  $\text{HB}^{\text{PW}}$ .



235

236 **Figure 3** Hydrogen bonds identified in the water-cellulose system: (a) criterion is defined as  
 237 distance shorter than 0.35 nm and angle smaller than 30°; (b) HB<sup>PP</sup>: hydrogen bonds between  
 238 cellulose and cellulose groups; (c) HB<sup>PW</sup>: hydrogen bonds between cellulose groups and water  
 239 molecules; (d) HB<sup>WW</sup>: hydrogen bonds between water and water molecules.

## 240 2.4. Mechanical testing

241 Generally, a hydrated polymeric system shows significant dependence on  
 242 moisture content regarding its mechanical properties. Here we mainly concentrate  
 243 on the Young's modulus. The Young's modulus of the hydrated polymer in this  
 244 paper is determined from the slope of the stress-strain relationship at small strains,  
 245 i.e. in the linear/elastic regime. Tensile tests are performed at different moisture  
 246 content in the  $x$ -,  $y$ - and  $z$ -directions respectively, where a linear uniaxial strain  
 247 ranging from 0 to 0.05 is applied at constant temperature  $T = 300$  K. The uniaxial  
 248 strain is imposed by changing the corresponding dimension of the simulation box  
 249 in the frame of a molecular dynamics run with a time span of 4 ns, while the  
 250 pressure in the other two dimensions is set to zero using a Nose-Hoover barostat.  
 251 The resulting tensile stress is extracted in a continuous fashion during the loading  
 252 procedure to obtain the stress-strain curve. Note that loading is conducted at  
 253 constant moisture content so that the measured quantity is the undrained Young's  
 254 modulus.

## 255 **2.5. Energy landscape**

256 To examine the interaction between the CN and water molecules, we calculate the  
257 potential energy landscape of the CN regarding CN-water interaction. In this  
258 scenario, the influence of the AC matrix on water is omitted and only the CN-water  
259 interaction is taken into consideration. At the selected cross section, a 400×400 grid  
260 mesh is generated, upon which the potential energy is calculated at each grid point  
261 by placing a probe water molecule. Note that the probed potential energy depends  
262 on the orientation of water molecules. Thus, energy minimization is carried out at  
263 each grid point before extracting the potential energy.

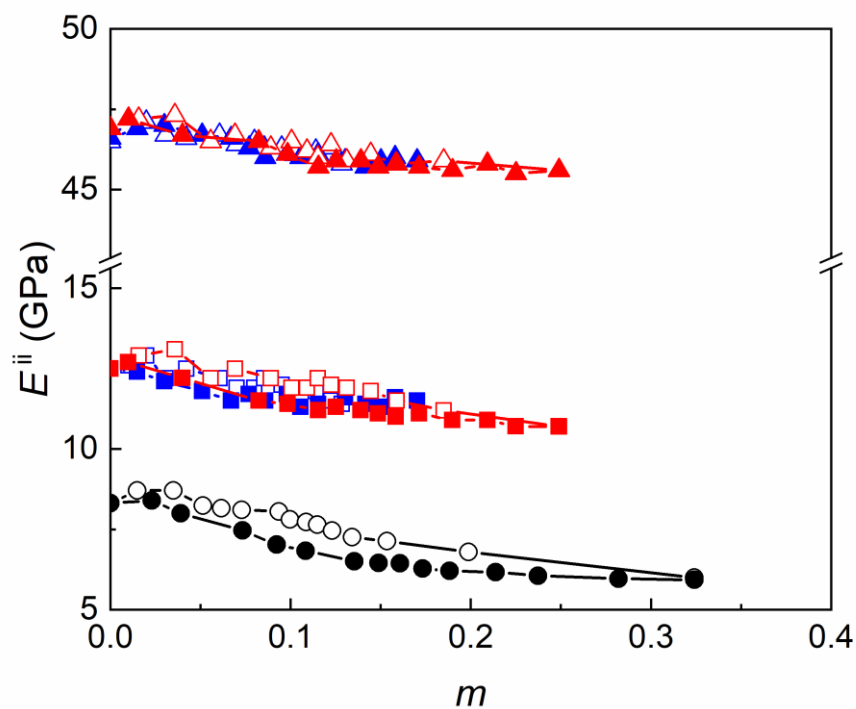
## 264 **3. Results and discussion**

### 265 **3.1 Role of CN on stiffness of ACC: reinforcing effect**

266 First, we study the influence of CN on the stiffness of the material. The  
267 Young's modulus is determined by tensile tests in MD simulation (Chen et al. 2018)  
268 at certain moisture contents. As the bulk AC model is isotropic, the Young modulus  
269 is taken as the average of Young moduli for the three principle directions. For the  
270 *partial-interaction* and *full-interaction* composites, the presence of CN introduces a  
271 mechanical anisotropy into the system, and two Young's moduli are considered:  
272 one in the longitudinal direction  $E^{zz}$  and the other in the transverse direction  $E^{tt}$   
273 (with the latter being calculated as the average of the moduli in x and y directions,  
274 i.e.,  $E^{tt}=(E^{xx}+E^{yy})/2$ ). The Young's moduli versus moisture content for the bulk  
275 AC, *partial-interaction* and *full-interaction* composites are compared in Figure 4. It  
276 shows that the two composites with/without CN-water interaction exhibit similar  
277 Young's moduli in both the longitudinal and transverse directions. This indicates  
278 that the CN influences the mechanical properties of the AC matrix mainly through  
279 the CN-AC interaction, while the role of CN-water interaction with regard to

280 mechanical behavior is less important. Therefore, with respect to the Young's  
 281 moduli, we will not distinguish the two composite models but only the reinforcing  
 282 effect.

283 Figure 4 shows that CN mainly reinforces the matrix in the longitudinal  
 284 direction by a factor of about 8.0 compared with the bulk AC. On the other hand,  
 285 the reinforcing effect in the transverse direction is limited to a factor of about 1.5.  
 286 Besides, we find both the Young's modulus of buck AC and composite materials  
 287 have strong dependence on the moisture content: Overall, the Young's modulus  
 288 decreases against the moisture content, except at the low moisture content range,  
 289 where the Young's modulus shows limited increase against the moisture content.



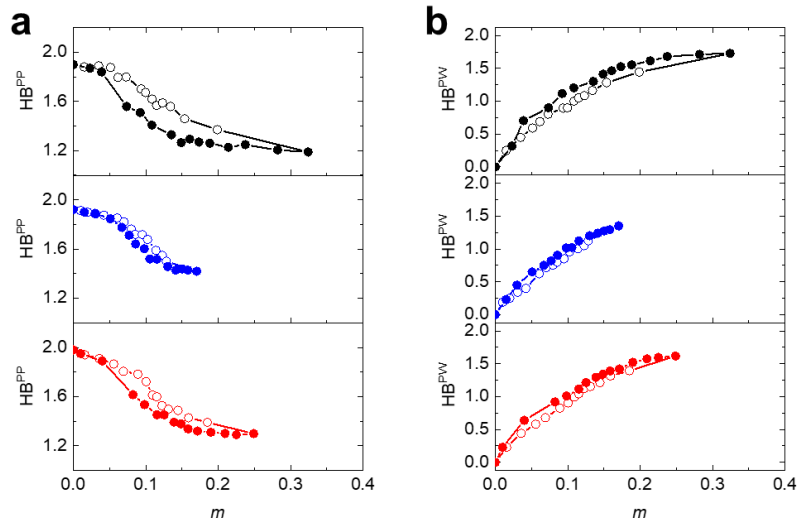
290

291 **Figure 4.** Relationship between Young modulus  $E$  and moisture content  $m$ . The black, blue and  
 292 red circles dots represent the bulk AC, *partial-interaction* composite and *full-interaction*  
 293 composite respectively. The open and closed symbols correspond to adsorption and desorption  
 294 data. The circles, squares and triangles represent the Young modulus of the bulk AC, transverse  
 295 Young modulus  $E^t$  and longitudinal Young modulus  $E^z$ , respectively.

296

297 The dependence of Young's modulus on moisture content for bulk polymers  
298 and composites can be understood by studying the occurrence of hydrogen bonds in  
299 the systems. Typically, there are three types of hydrogen bonds in a hydrated  
300 polymer system: polymer-to-polymer hydrogen bonds  $HB^{PP}$ , polymer-to-water  
301 hydrogen bonds  $HB^{PW}$  and water-to-water hydrogen bonds  $HB^{WW}$ , among which  
302  $HB^{PP}$  and  $HB^{PW}$  are particularly instructive about internal structural rearrangements  
303 of polymer chains due to water sorption (Chen et al. 2018). Here we plot in Figure 5  
304 the dependence of polymer related hydrogen bonds, i.e.,  $HB^{PP}$  and  $HB^{PW}$  in the bulk  
305 AC and in the matrix of the composites upon moisture content change. We can see  
306 that  $HB^{PP}$  decreases against the moisture content for all three models while  $HB^{PW}$   
307 increases. This is mainly attributed to the swelling of AC upon water sorption. As  
308 water gets adsorbed into the interchain space pushing away the neighboring  
309 cellulose chains, the interchain distance increases and some  $HB^{PP}$  break, leading to  
310 the mechanical weakening of the system. This explains the softening, or decrease of  
311 Young's modulus, of the system upon water sorption.

312 Of interest, we also observe, in Figure 4, a mild increase of Young's modulus  
313 at very low moisture content upon water sorption. Concurrently, we see in Figure 5  
314 that the number of  $HB^{PP}$  barely decreases over this low moisture content range for  
315 all three models. This indicates that most of the water molecules adsorbed at low  
316 RH fill in the initially existing pores of the dry AC and only the water molecules  
317 adsorbed afterwards result in more significant swelling of the polymer and breaking  
318 of  $HB^{PP}$ . With the number of  $HB^{PP}$  almost constant and the configuration of AC  
319 almost unaffected, the Young's modulus of the slightly hydrated system is higher  
320 than the dry state as the initial porosity has been filled by the water molecules  
321 without weakening the AC skeleton. This explains the mild increase of Young's  
322 modulus versus moisture content at low RH shown by Figure 4.



323

324 **Figure 5** Dependence of number of (a) polymer-to-polymer hydrogen bonds ( $HB^{PP}$ ) and  
 325 water-to-polymer hydrogen bonds ( $HB^{PW}$ ) on moisture content. The results from three systems with bulk  
 326 AC model, *partial-interaction* model and *full-interaction* model result in top (black), middle (blue)  
 327 and bottom (red) panels, Adsorption and desorption results are plotted using open and closed  
 328 circles respectively.

329 Now we consider the mechanical effect of adding CN reinforcement into the  
 330 AC matrix. We find that, for the composite, the decrease in Young's modulus  
 331 versus moisture content is more limited for transverse directions compared to the  
 332 bulk AC (and even less for longitudinal direction). As the breaking of  $HB^{PP}$  relies  
 333 on swelling of the AC matrix, a more limited swelling of AC due to the  
 334 reinforcement of CN in the composite leads to fewer breakage of  $HB^{PP}$  (Figure 5),  
 335 which finally results in less variation of Young modulus. Thus, we see less moisture  
 336 content, less swelling, less breakage of  $HB^{PP}$  and less weakening effect at saturation.

337 Hysteresis in Young's modulus against moisture content is observed mainly for  
 338 the bulk AC. A smaller hysteresis is observed for the transverse directions, while  
 339 hysteresis for the longitudinal direction is very limited. The hysteresis in Young  
 340 modulus arises from the hysteresis in  $HB^{PP}$ , which undergoes a different sequence  
 341 along the adsorption and desorption branches. We can see clearly in Figure 5 (a)  
 342 that there are more  $HB^{PP}$  in adsorption branch, which corresponds to higher  
 343 Young's modulus compared to that in the desorption branch with the same moisture

344 content. i.e., the hysteretic modulus dependence on moisture content. The smaller  
345 hysteresis for the composites can be attributed to two major reasons: One is the less  
346 breaking of HB<sup>PP</sup> due to less swelling caused by the reinforcing effect, which can be  
347 confirmed in Figure 5 (a) that there are more HB<sup>PP</sup> left at saturation for the two  
348 composite models. The other is the mixing fact: Young's modulus of the composite  
349 is strongly affected by CN, which is a non-sorptive and mechanically reversible  
350 reinforcement. With the presence of CN, the mechanical properties of the composite  
351 are expected to be less hysteretic compared to that of the matrix.

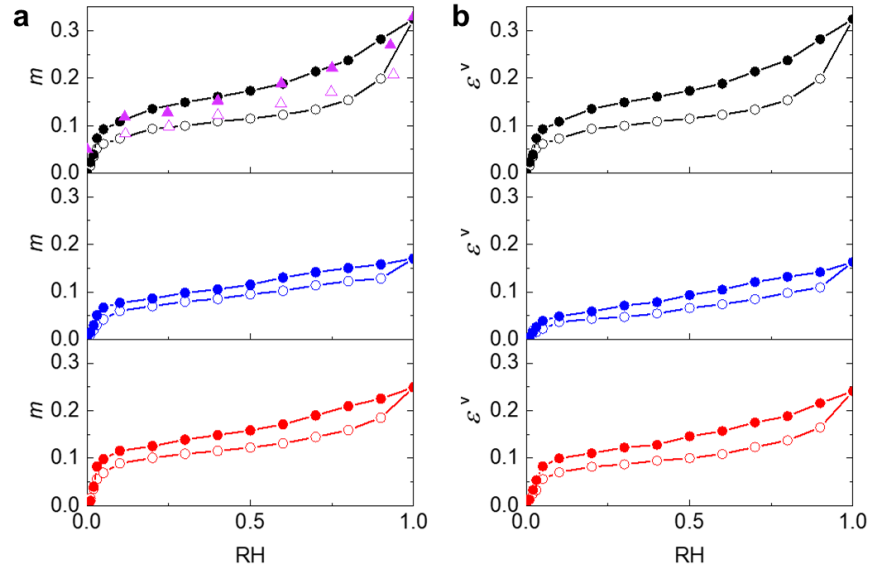
### 352 **3.2. Role of CN on the sorption and strain isotherms**

353 Adsorption and desorption isotherms are plotted in Figure 6 (a). Moisture  
354 content  $m$  in the three cases is defined as  $m = m^W/m^{AC}$ , where  $m^W$  and  $m^{AC}$  are  
355 masses of water molecules and AC respectively. Generally, moisture content is  
356 defined as the ratio between the mass of water uptake and the total mass of  
357 composite. However, as water molecules are only adsorbed in the AC matrix,  
358 including its interface with CN, it is more insightful to exclude the mass of CN from  
359 the denominator. This definition allows us to directly compare the sorption behavior  
360 with/without CN.

361 The sorption isotherms of the three models are of type II according to the  
362 classification of IUPAC (International Union of Pure and Applied Chemistry)  
363 (Thommes et al. 2015). That is, the moisture content  $m$  increases sharply at low RH,  
364 slowly at medium RH range and then sharply again at large RH. Sorption hysteresis,  
365 which persists throughout the RH range from 0 to 1.0, is present in the three  
366 systems - although the size of the hysteresis loop differs. The sorption isotherms of  
367 the bulk AC model are compared to the experimental one (Mihryan et al. 2004),  
368 with a shift of  $m = +0.05$  to account for the presence of residual i.e., non-desorbable,



369 water due to experimental difficulties of attaining dry conditions or unavoidable  
 370 partial rehydration upon weighing (Chen et al. 2018). The simulated sorption  
 371 isotherms agree well with the experimental data.



372

373 **Figure 6.** (a) Sorption isotherms and (b) Strain isotherms of the three systems with bulk AC  
 374 model, *partial-interaction* model and *full-interaction* model results in top (black), middle (blue)  
 375 and bottom (red) panels, at  $T = 300$  K. Adsorption and desorption results from simulations are  
 376 plotted using open and closed circles respectively. Experimental adsorption and desorption  
 377 isotherms of pure AC are plotted using open and closed (purple) triangles (Mihrianyan et al. 2004).

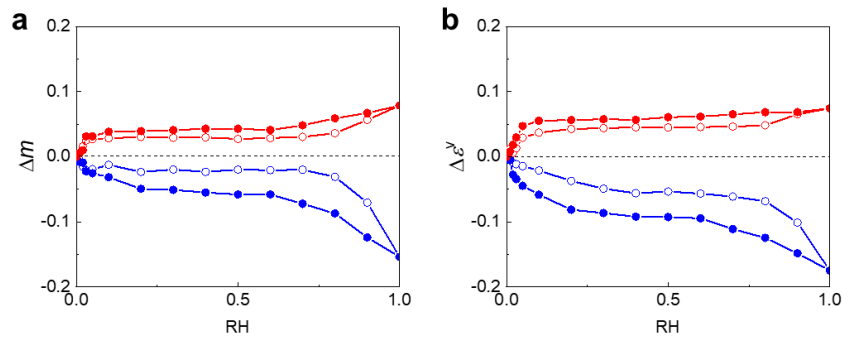
378 The strain isotherms of the three models are plotted in Figure 6 (b). By analogy  
 379 with the definition of moisture content used above, the volumetric strain of AC is  
 380 defined as  $\epsilon^V = \Delta V^{AC} / V_0^{AC}$ , where  $V_0^{AC}$  and  $\Delta V^{AC}$  are the initial and  
 381 incremental volumes of AC matrix. The strain isotherms exhibit shapes similar to  
 382 the ones of the sorption isotherms with a significant hysteresis. Both types of  
 383 composites show a lower moisture content and swelling strain, indicating that the  
 384 CN manifests its reinforcing effect not only in the modulus as discussed before but  
 385 also in the sorption process. Moreover, the different sorption and strain isotherms of  
 386 the *partial-interaction* and *full-interaction* composites demonstrate that the CN-  
 387 water interaction also affects the results. These features indicate that CN plays

388 multiple roles in the sorption process which calls for additional  
389 characterization/investigation.

390 To study the reinforcing effect of CN on the sorption and swelling isotherms  
391 (i.e. versus RH), we plot the differential moisture content  $\Delta m$  and differential  
392 volumetric strain  $\Delta \varepsilon^V$  (blue circles) in Figure 7 (a) between *partial-interaction*  
393 composite and bulk AC. These differences are defined as:  $\Delta m = m|_{\text{partial}} - m|_{\text{AC}}$  and  
394  $\Delta \varepsilon^V = \varepsilon^V|_{\text{partial}} - \varepsilon^V|_{\text{AC}}$ , where  $m|_{\text{partial}}$ ,  $\varepsilon^V|_{\text{partial}}$ ,  $m|_{\text{AC}}$  and  $\varepsilon^V|_{\text{AC}}$  are the moisture content  
395 and volumetric strain of the *partial-interaction* composite and bulk AC respectively.  
396 We see a significant reduction of the moisture content and volumetric strain, which  
397 can be attributed to the reinforcing effect of CN. As the swelling of matrix is  
398 constrained by the CN, there is less additional inter-chain space created in the  
399 matrix to accommodate water molecules. Thus, it becomes harder for water  
400 molecules to be adsorbed into the matrix at given RH and moisture content drops in  
401 the *partial-interaction* composite. As shown in Figure 7, the reduction of moisture  
402 content and of volumetric strain in desorption branches is greater than in the  
403 adsorption branches. This means that the sorption and strain hysteresis in the  
404 *partial-interaction* composite is compressed by the CN. We recall that, in the  
405 *partial-interaction* composite, the CN does not impose any direct impact on  
406 sorption as the CN-water interaction is turned off. We conclude that the reduction in  
407 moisture content in the *partial-interaction* composite, together with the compressed  
408 sorption hysteresis, is caused by the mechano-sorptive effect. This means that the  
409 sorption behavior is influenced by the mechanical conditions due to the coupling  
410 between sorption and deformation.

411 Apart from the reinforcing effect, CN is also expected to directly influence on  
412 the sorption process through the CN-water interaction. To study this effect, we plot  
413 the differential moisture content  $\Delta m$  and volumetric strain  $\Delta \varepsilon^V$  between the *full* and

414 *partial-interaction* models in Figure 7. The differences are defined as:  $\Delta m = m_{\text{full}} -$   
 415  $m_{\text{partial}}$  and  $\Delta \varepsilon^V = \varepsilon^V_{\text{full}} - \varepsilon^V_{\text{partial}}$  where  $m_{\text{full}}$  and  $\varepsilon^V_{\text{full}}$  are moisture content and  
 416 volumetric strain of the *full-interaction* composite. Figure 7 shows that the  
 417 difference values are positive (red circles), which means that the moisture content  
 418 and the swelling become larger when the CN-water interaction is switched on.  
 419 Moreover, this enhancement in sorption leads to larger sorption and deformation  
 420 hysteresis. Because of the attraction of CN, more water molecules get adsorbed into  
 421 the AC matrix, therefore inducing a larger swelling of the matrix (with more broken  
 422 HB<sup>PP</sup>). Thus, there are more hydroxyl groups on the polymer chains exposed as  
 423 additional sorption sites for water molecules which finally contribute to the  
 424 hysteresis of the system.

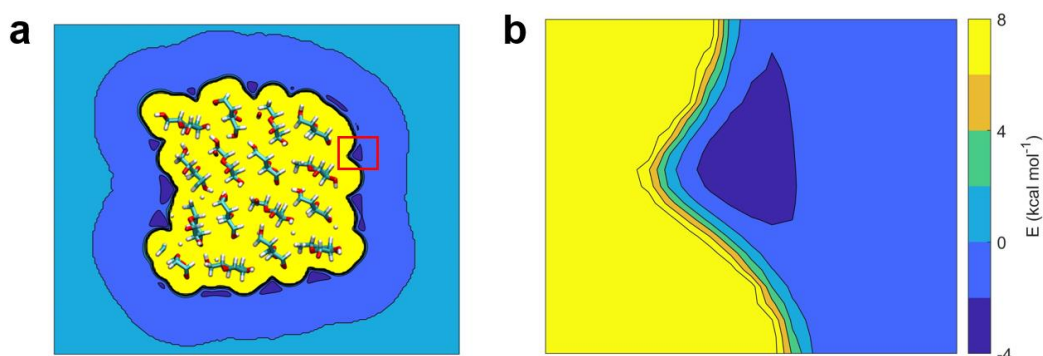


425

426 **Figure 7.** Differential (a) moisture content  $\Delta m$  and (b) volumetric strain  $\Delta \varepsilon^V$  between the *partial-*  
 427 *interaction* composite and AC (blue) and between the *full-interaction* composite and *partial-*  
 428 *interaction* composite (red) as functions of RH. Open and closed circles represent adsorption and  
 429 desorption respectively.

430 The difference of sorption and swelling between the two composites arises thus  
 431 from the CN-water interaction. The strength of CN-water interaction can be  
 432 characterized by looking at the energy landscape. As shown in Figure 8 (a), the  
 433 potential energy within CN is positive, higher than  $8.0 \text{ kcal.mol}^{-1}$ . This means that

434 penetration of water molecules into the CN involves a large energy cost that is  
435 unlikely to happen. The energy landscape outside the CN corresponds to negative  
436 values, which means that water molecules minimize the system energy by  
437 approaching CN. Figure 8 (b) also shows that the most favorable adsorption sites  
438 are located at the concave surface, where the energy well is enhanced by the  
439 surrounding hydroxyl groups at the CN surface.



440

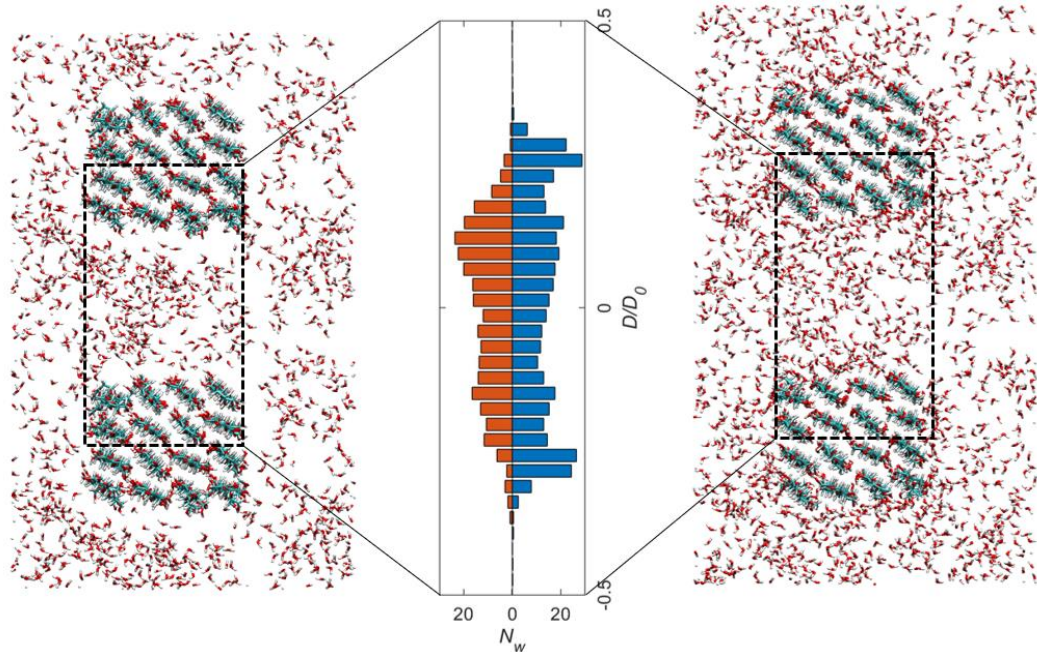
441 **Figure 8.** (a) Potential energy landscape of water molecules around the CN; (b) zoom-in of the  
442 energy landscape within the red box depicted in (a).

443 The direct influence of CN on sorption can also be probed by looking at water  
444 distributions in the matrix. Snapshots of water distribution in the *partial-interaction*  
445 and *full-interaction* composites at RH=1.0 are shown in Figure 9. The AC matrix is  
446 omitted in the plot. It shows that the water distributions in the matrix far enough  
447 from the CN are similar in the two cases. The main difference is seen at the CN/AC  
448 interface. For the *partial-interaction* composite, there is a very limited number of  
449 water molecules adsorbed at the interface, while water molecules tend to cluster at  
450 the interface for the *full-interaction* composite. This impression built on the  
451 snapshots is confirmed by checking water distributions within the slit formed  
452 between two CNs, which is displayed in the middle of Figure 9. The histogram of  
453 water distributions is acquired by averaging  $2 \times 10^6$  MD timesteps upon sorption  
454 equilibrium at RH = 1.0. The data shown in Figure 9 are acquired over a black  
455 dashed box with dimensions  $2.5 \times 4.9 \text{ nm}^2$ . It shows that there are very few water

456 molecules at the interface for the *partial-interaction* model and the moisture content  
457 increases gradually away from the interface until reaching a plateau. Though the  
458 plateau is not flat and the density profile is not symmetric because of the  
459 heterogeneous porous structure of AC matrix at such a finite size, we see that the  
460 interface exhibits a hydrophobic behavior. Moreover, the large stiffness of CN  
461 together with the CN-AC interaction makes the AC adjacent to CN stiffer and hard  
462 to swell, resulting in a reduction of the moisture content in the stiffened AC matrix  
463 region.

464       When turning to the *full-interaction* composite, this composite leads to water  
465 molecules clustering at the interface of the CN. The water density profile exhibits a  
466 peak at the interface. In this case, the CN-water interaction, as a competing factor  
467 against the reinforcing effect, comes into play. CN attracts water molecules to the  
468 interface and enhances water sorption. Though the reinforcing effect is still present  
469 and hinders water sorption, it shows in our case that the CN-water interaction is so  
470 strong at the interface that it dominates the sorption behavior there. In contrast, at  
471 the middle of the slit – i.e. far from the interface – both the reinforcing effect and  
472 the CN-water attraction diminish so that no significant difference in water  
473 distributions is found between the two cases. Similar enhanced water sorption at the  
474 reinforcement/matrix interface was reported previously by Kulasinski et al  
475 (Kulasinski et al. 2017), who attributed the enhanced sorption to the higher porous  
476 structure of the interface because of the structural mismatch between the  
477 reinforcement and matrix. However, considering that the mentioned structural  
478 mismatch and higher porous structure of the interface depend merely on the  
479 reinforcement/matrix interaction (which is the same for the *partial-interaction* and  
480 *full-interaction* composites), the explanation of a different interface structure does  
481 not hold. The comparison between the two different composites in this work reveals

482 that the enhanced water sorption at the interface is mainly due to the CN-water  
483 interaction rather than the microstructure of the interface due to structural mismatch.



484

485 **Figure 9.** Typical molecular configurations of water molecules distributed in the matrix of *partial-*  
486 *interaction* (left) and *full-interaction* (right) composites projected along the longitudinal direction.  
487 The plot of matrix is omitted for better visualization of water distribution. The water density  
488 histograms within the black dashed boxes are plotted in the *middle*, with the red and blue data  
489 representing the *partial-interaction* and *full-interaction* composites respectively.  $D_0 = 4.9$  nm is  
490 the length of the box.

491 Two competing mechanisms have been characterized so far in this subsection  
492 regarding the impact of CN on sorption and swelling behavior of the composites:  
493 the reinforcing effect of CN constrains the sorption and swelling, and the CN-water  
494 attraction enhances the sorption and swelling. The question naturally arises that  
495 what is the overall impact of CN on the sorption and swelling of the composite? For  
496 the current configuration studied in this paper, the overall effect of CN is  
497 constraining the sorption and swelling. This can be easily seen from Figure 6 by  
498 comparing the isotherms of bulk AC (top panel) and the full-interaction composite  
499 (bottom panel) as the magnitude of sorption/strain isotherm for the full-interaction  
500 composite is smaller than that for the bulk AC. This means that, for our

501 configuration, the constraining mechanism outperforms the enhancing mechanism.  
502 However, one must note the overall effect of CN should heavily depend on the  
503 composite configuration. One can expect that, with a different configuration  
504 (different volume fraction of CN, for instance), the enhancing mechanism may  
505 outperform the constraining mechanism, leading to an opposite overall effect  
506 compared to the configuration in this paper. As we mentioned in the Introduction,  
507 the overall effect of CN can be either enhancing or constraining according to  
508 experiments. The underlying reasons of this inconsistency between different  
509 experiments remain unknown. With the characterization of the enhancing and  
510 constraining mechanisms, we believe that this inconsistency could be explained by  
511 the competition of the two mechanisms.

### 512 **3.3. Role of CN on swelling coefficients**

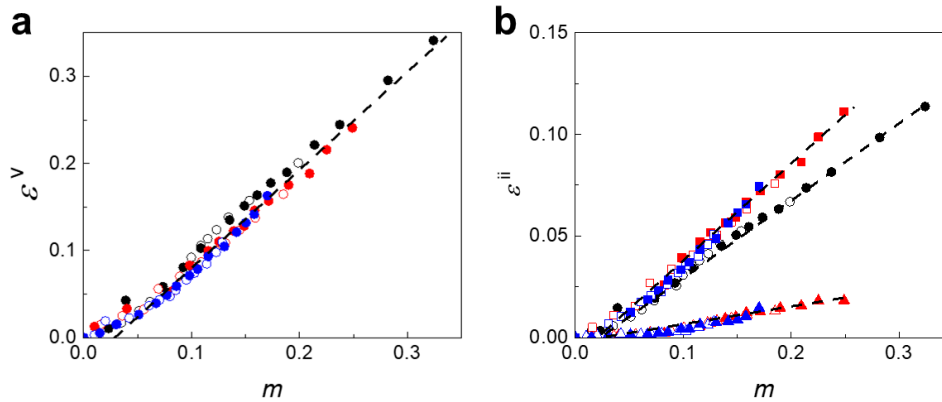
513 In the adsorption/strains isotherms, lower/higher strains correspond to  
514 lower/higher moisture contents, indicating a monotonic relationship between  
515 moisture content and strain. This relationship is confirmed by plotting strain versus  
516 moisture content which shows a linear relationship with the moisture content for all  
517 the three systems, see Figure 10(a). Also, the data for adsorption and desorption  
518 collapse into a single relationship, meaning we get a unique  $m \sim \varepsilon^V$  curve regardless  
519 of the presence of CN and the moisture history. In effect, water gets adsorbed into  
520 AC and creates the space for its accommodation by exerting repulsive forces on the  
521 polymer chains. This additional space created by the adsorbed water molecules is at  
522 the origin of the sorption-induced swelling. The same coupling physics persists  
523 throughout adsorption and desorption and remains the same in the different systems.  
524 As a result, all the data collapse on a single relationship on the  $m \sim \varepsilon^V$  curve.

525 As CN introduces mechanical anisotropy into the composite, we check the  
526 uniaxial swelling behaviors of the three systems. Similar to the strategy used in our  
527 study of Young modulus, we define the uniaxial strain of bulk AC model as the  
528 average uniaxial strain of all three directions because of its isotropy. For the  
529 composites, we look at the longitudinal strain  $\varepsilon^{zz}$  and transverse strain  $\varepsilon^{tt}$  of the AC  
530 matrix, where  $\varepsilon^{tt}$  is calculated by the average of strain in two transverse directions,  
531 i.e.,  $\varepsilon^{tt} = (\varepsilon^{xx} + \varepsilon^{yy}) / 2$ . The uniaxial strain of two composite systems are compared  
532 with the bulk AC in Figure 10(b). The uniaxial swelling coefficient is determined  
533 by the slope of the strain versus moisture content curve. It shows that there is no  
534 significant difference in the swelling coefficient for *partial-interaction* and *full-*  
535 *interaction* composites. Therefore, we only discuss in what follows the reinforcing  
536 effect and compare the uniaxial swelling coefficient of the bulk AC and the  
537 composites.

538 The swelling coefficients in the longitudinal and transverse directions of the  
539 composites are equal to 0.10 and 0.48. On the other hand, the swelling coefficient  
540 for bulk AC is 0.35. The small swelling coefficient in longitudinal direction of the  
541 composite compared to the bulk AC is attributed to the strong reinforcing effect of  
542 CN in the longitudinal direction. By contrast, the swelling coefficient of the  
543 composite in transverse direction is found to be higher than the uniaxial swelling  
544 coefficient of the bulk AC. We can explain this by the fact that the relationship  
545 between volumetric strain and moisture content is unique as the same moisture  
546 content leads to the same change of volume, thus the same volumetric strain. Since  
547 the swelling in the composite along the longitudinal direction is restrained by the  
548 reinforcing effect of CN, this strain will be much lower than 1/3 of the volumetric  
549 strain (which would be the case in an isotropic material). As a result, to obtain the  
550 same volumetric strain, the strain along the transverse directions will be higher than



551 1/3 of the volumetric strain, causing a swelling coefficient in transverse directions  
 552 higher than that of bulk AC. We may conclude that the swelling coefficients, i.e. the  
 553 amount of strain with increasing moisture content, only depends on the reinforcing  
 554 effect as no difference between the two composites is seen.



555

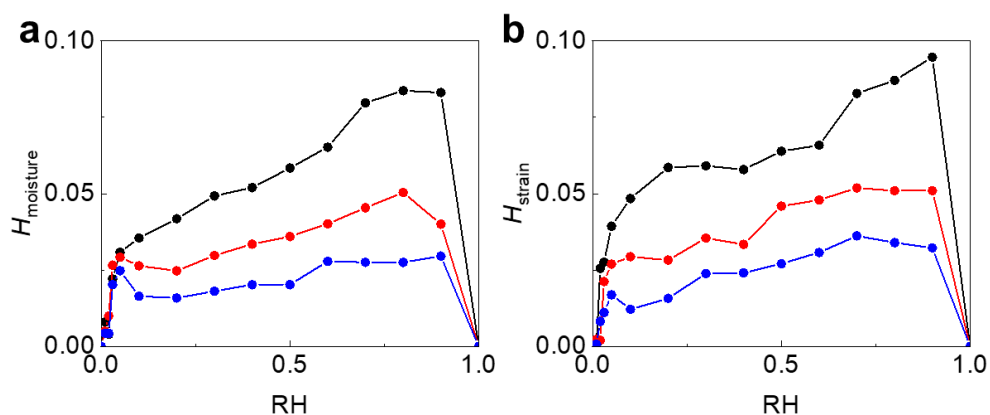
556 **Figure 10.** Relationship between (a) volumetric strain and (b) uniaxial strain and moisture content  
 557  $m$ . Black, blue and red circles represent the bulk AC, *partial-interaction* and *full-interaction*  
 558 composites respectively. The open and closed symbols are the adsorption and desorption data. The  
 559 circles, squares and triangles represent volumetric strain  $\epsilon^V$ , transverse strain  $\epsilon^{tt}$  and longitudinal  
 560 strain  $\epsilon^{zz}$  respectively. The black dashed lines are drawn as guides to the eye.

### 561 3.4. Influence of CN on hysteresis in sorption and swelling isotherms

562 Hysteresis is characterized by the difference of moisture content/strain between  
 563 the desorption and adsorption branch, i.e.,  $H_{\text{moisture}}=m_{\text{de}} - m_{\text{ad}}$  and  $H_{\text{strain}}=\epsilon_{\text{de}}^V - \epsilon_{\text{ad}}^V$ ,  
 564 where  $m_{\text{de}}$ ,  $m_{\text{ad}}$ ,  $\epsilon_{\text{de}}^V$  and  $\epsilon_{\text{ad}}^V$  are moisture content and volumetric strain in the  
 565 desorption and adsorption branch respectively. The sorption and strain hysteresis of  
 566 the three systems are plotted in Figure 11. A comparison between the bulk AC  
 567 (black circles) and *partial-interaction* composite (blue circles) clearly shows that  
 568 the hysteresis shrinks because of the reinforcing effect of CN in both sorption and  
 569 strain:  $H_{\text{moisture}}$  and  $H_{\text{strain}}$  are lower in the *partial-interaction* composite throughout

570 the entire RH range. According to (Chen et al. 2018), the hysteresis relies on the  
571 breakage of HB<sup>PP</sup> to expose the hydroxyl groups on polymer chains as additional  
572 sorption sites for water molecules. The presence of CN constrains the deformation  
573 of the AC matrix thus leading to less breakage of HB<sup>PP</sup> as shown in Figure 5. As a  
574 result, the hysteresis is greatly diminished by the mechanical reinforcing effect of  
575 CN.

576 Comparison between the *partial-interaction* and *full-interaction* models shows  
577 that hysteresis in both sorption and strain isotherms is enlarged by the CN-water  
578 interaction. As discussed in Section 3.1, the CN-water interaction induces a  
579 hydrophilic interface, where the sorption is greatly enhanced and results in a  
580 clustering of water molecules. As a result, the AC matrix swells more to  
581 accommodate the increased moisture content which leads to a larger number of  
582 HB<sup>PP</sup> breakage (Figure 5). This additional breakage of HB<sup>PP</sup> finally contributes to  
583 the enlarged sorption and deformation hysteresis. On the other hand, the hysteresis  
584 of the *full-interaction* composite is smaller than that of the bulk AC, although larger  
585 than the *partial-interaction* composite. This means that the reinforcing effect of CN  
586 is more dominating for the current configure regarding hysteresis.



587

588 **Figure 11.** Hysteresis of three systems in (a) moisture content and (b) strain. The black, blue and  
 589 red circles represent the bulk AC, *partial-interaction* composite and *full-interaction* composite  
 590 respectively.

## 591 4. Conclusion

592 ● This work addresses the role of cellulose nanocrystals (CN) in the coupling  
 593 between sorption and deformation of CN-based nanocomposites and the  
 594 related hysteresis phenomenon. With the help of hybrid GCMC/MD  
 595 simulations, three samples are considered: pure amorphous cellulose (AC),  
 596 CN/AC composite without CN-water interaction and CN/AC composite  
 597 with CN-water interaction. By comparison between these different systems,  
 598 we characterize the two major roles played by CN in the coupling behavior.  
 599 One is the mechanical reinforcing effect through the CN-AC interaction,  
 600 which stiffens the matrix and limits the swelling. As a result, water  
 601 sorption in the AC matrix is hindered. Moreover, the sorption and strain  
 602 hysteresis shrink because of the reduced breakage of hydrogen bonds due  
 603 to the limited swelling. The other effect is the sorption enhancing effect  
 604 through CN-water interaction, which attracts water toward the CN/AC

605 interface – which enhances sorption at the interface and increases the  
606 swelling. Accordingly, the hysteresis in both sorption and strain is enlarged  
607 due to sufficient hydrogen bond breaking. The sorption and swelling of the  
608 composite result from the competition of the two factors. Other aspects  
609 related to the two roles are also examined. We find anisotropic swelling  
610 and mechanical weakening behavior of the composite upon sorption  
611 because of the orientation of CN. Moreover, the mechanism of sorption at  
612 the CN/AC interface is characterized.

613 The findings presented in this work deepen our understanding of sorption and  
614 swelling of CN-reinforced nanocomposites and related hysteresis. The two  
615 competing roles of CN can be used for composite material design to tailor targeted  
616 coupled behaviors. More generally, as most works regarding the sorption-induced  
617 deformation in nonporous materials concentrate mainly on homogenous media, we  
618 expect that this work can bring attention to the sorption-induced deformation and  
619 related hysteresis of heterogenous nanocomposites which widely exist in nature.

620

## 621 **Acknowledgements**

622 The authors acknowledge the support of the Swiss National Science  
623 Foundation (SNSF) (no. 143601).

## 624 **References**

625 Anfara VA, Brown KM, Mangione TL (2002) Qualitative Analysis on Stage:  
626 Making the Research Process More Public. *Educ Res* 31:28–38.  
627 <https://doi.org/10.3102/0013189X031007028>

628 Anglès MN, Dufresne A (2001) Plasticized Starch/Tunicin Whiskers  
629 Nanocomposite Materials. 2. Mechanical Behavior. *Macromolecules*  
630 34:2921–2931. <https://doi.org/10.1021/ma001555h>

- 631 Anglès MN, Dufresne A (2000) Plasticized Starch/Tunicin Whiskers  
632 Nanocomposites. 1. Structural Analysis. *Macromolecules* 33:8344–8353.  
633 <https://doi.org/10.1021/ma0008701>
- 634 Azizi Samir MAS, Alloin F, Sanchez J-Y, Dufresne A (2004) Cellulose  
635 nanocrystals reinforced poly(oxyethylene). *Polymer (Guildf)* 45:4149–4157.  
636 <https://doi.org/10.1016/j.polymer.2004.03.094>
- 637 Barkas WW (1939) Wood Water Relationships. IV. The Swelling and Shrinkage  
638 of Wood in Relation to its Mechanical Properties. *J Chem Inf Model* 388.  
639 <https://doi.org/10.1017/CBO9781107415324.004>
- 640 Blanco A, Monte MC, Campano C, et al (2018) Nanocellulose for Industrial Use.  
641 In: *Handbook of Nanomaterials for Industrial Applications*. Elsevier, pp 74–  
642 126
- 643 Brown RM (2004) Cellulose structure and biosynthesis: What is in store for the  
644 21st century? *J Polym Sci Part A Polym Chem* 42:487–495.  
645 <https://doi.org/10.1002/pola.10877>
- 646 Brown RM (1996) The Biosynthesis of Cellulose. *J Macromol Sci Part A*  
647 33:1345–1373. <https://doi.org/10.1080/10601329608014912>
- 648 Charlier L, Mazeau K (2012) Molecular Modeling of the Structural and  
649 Dynamical Properties of Secondary Plant Cell Walls: Influence of Lignin  
650 Chemistry. *J Phys Chem B* 116:4163–4174.  
651 <https://doi.org/10.1021/jp300395k>
- 652 Chen M, Coasne B, Derome D, Carmeliet J (2020) Coupling of sorption and  
653 deformation in soft nanoporous polymers: Molecular simulation and  
654 poromechanics. *J Mech Phys Solids* 137:103830.  
655 <https://doi.org/10.1016/j.jmps.2019.103830>
- 656 Chen M, Coasne B, Guyer R, et al (2018) Role of hydrogen bonding in hysteresis  
657 observed in sorption-induced swelling of soft nanoporous polymers. *Nat*  
658 *Commun* 9:3507. <https://doi.org/10.1038/s41467-018-05897-9>
- 659 Chen M, Coasne B, Guyer R, et al (2019a) Molecular Simulation of Sorption-  
660 Induced Deformation in Atomistic Nanoporous Materials. *Langmuir*  
661 35:7751–7758. <https://doi.org/10.1021/acs.langmuir.9b00859>
- 662 Chen W, Lickfield GC, Yang CQ (2004) Molecular modeling of cellulose in  
663 amorphous state. Part I: model building and plastic deformation study.  
664 *Polymer (Guildf)* 45:1063–1071.  
665 <https://doi.org/10.1016/j.polymer.2003.11.020>
- 666 Chen, Zhang, Shomali, et al (2019b) Wood–Moisture Relationships Studied with  
667 Molecular Simulations: Methodological Guidelines. *Forests* 10:628.  
668 <https://doi.org/10.3390/f10080628>
- 669 de Mesquita JP, Donnici CL, Teixeira IF, Pereira F V. (2012) Bio-based  
670 nanocomposites obtained through covalent linkage between chitosan and

- 671 cellulose nanocrystals. *Carbohydr Polym* 90:210–217.  
672 <https://doi.org/10.1016/j.carbpol.2012.05.025>
- 673 Derome D, Griffa M, Koebel M, Carmeliet J (2011) Hysteretic swelling of wood  
674 at cellular scale probed by phase-contrast X-ray tomography. *J Struct Biol*  
675 173:180–190. <https://doi.org/10.1016/j.jsb.2010.08.011>
- 676 Derome D, Rafsanjani A, Patera A, et al (2012) Hygromorphic behaviour of  
677 cellular material: hysteretic swelling and shrinkage of wood probed by phase  
678 contrast X-ray tomography. *Philos Mag* 92:3680–3698.  
679 <https://doi.org/10.1080/14786435.2012.715248>
- 680 Favier V, Chanzy H, Cavaille JY (1995) Polymer Nanocomposites Reinforced by  
681 Cellulose Whiskers. *Macromolecules* 28:6365–6367.  
682 <https://doi.org/10.1021/ma00122a053>
- 683 Gomes TCF, Skaf MS (2012) Cellulose-Builder: A toolkit for building crystalline  
684 structures of cellulose. *J Comput Chem* 33:1338–1346.  
685 <https://doi.org/10.1002/jcc.22959>
- 686 Habibi Y, Goffin A-L, Schiltz N, et al (2008) Bionanocomposites based on  
687 poly( $\epsilon$ -caprolactone)-grafted cellulose nanocrystals by ring-opening  
688 polymerization. *J Mater Chem* 18:5002. <https://doi.org/10.1039/b809212e>
- 689 Habibi Y, Lucia LA, Rojas OJ (2010a) Cellulose Nanocrystals: Chemistry, Self-  
690 Assembly, and Applications. *Chem Rev* 110:3479–3500.  
691 <https://doi.org/10.1021/cr900339w>
- 692 Habibi Y, Lucia LA, Rojas OJ (2010b) Cellulose Nanocrystals: Chemistry, Self-  
693 Assembly, and Applications. *Chem Rev* 110:3479–3500.  
694 <https://doi.org/10.1021/cr900339w>
- 695 Hofstetter K, Hinterstoisser B, Salmén L (2006) Moisture uptake in native  
696 cellulose – the roles of different hydrogen bonds: a dynamic FT-IR study  
697 using Deuterium exchange. *Cellulose* 13:131–145.  
698 <https://doi.org/10.1007/s10570-006-9055-2>
- 699 Huber T, Müssig J, Curnow O, et al (2012) A critical review of all-cellulose  
700 composites. *J Mater Sci* 47:1171–1186. <https://doi.org/10.1007/s10853-011-5774-3>
- 702 Kafy A, Akther A, Shishir MIR, et al (2016) Cellulose nanocrystal/graphene  
703 oxide composite film as humidity sensor. *Sensors Actuators A Phys*  
704 247:221–226. <https://doi.org/10.1016/j.sna.2016.05.045>
- 705 Karim Z, Mathew AP, Grahn M, et al (2014) Nanoporous membranes with  
706 cellulose nanocrystals as functional entity in chitosan: Removal of dyes from  
707 water. *Carbohydr Polym* 112:668–676.  
708 <https://doi.org/10.1016/j.carbpol.2014.06.048>
- 709 Kulasinski K, Derome D, Carmeliet J (2017) Impact of hydration on the  
710 micromechanical properties of the polymer composite structure of wood

- 711 investigated with atomistic simulations. *J Mech Phys Solids* 103:221–235.  
712 <https://doi.org/10.1016/j.jmps.2017.03.016>
- 713 Kulasinski K, Keten S, Churakov S V., et al (2014) A comparative molecular  
714 dynamics study of crystalline, paracrystalline and amorphous states of  
715 cellulose. *Cellulose* 21:1103–1116. [https://doi.org/10.1007/s10570-014-](https://doi.org/10.1007/s10570-014-0213-7)  
716 [0213-7](https://doi.org/10.1007/s10570-014-0213-7)
- 717 Kulasinski K, Salmén L, Derome D, Carmeliet J (2016) Moisture adsorption of  
718 glucomannan and xylan hemicelluloses. *Cellulose* 23:1629–1637.  
719 <https://doi.org/10.1007/s10570-016-0944-8>
- 720 Liu C, Jin R-N, Ouyang X, Wang Y-G (2017) Adsorption behavior of  
721 carboxylated cellulose nanocrystal—polyethyleneimine composite for  
722 removal of Cr(VI) ions. *Appl Surf Sci* 408:77–87.  
723 <https://doi.org/10.1016/j.apsusc.2017.02.265>
- 724 Luzar A, Chandler D (1993) Structure and hydrogen bond dynamics of water–  
725 dimethyl sulfoxide mixtures by computer simulations. *J Chem Phys*  
726 98:8160–8173. <https://doi.org/10.1063/1.464521>
- 727 Luzar A, Chandler D (1996) Hydrogen-bond kinetics in liquid water. *Nature*  
728 379:55–57. <https://doi.org/10.1038/379055a0>
- 729 Maréchal Y, Chanzy H (2000) The hydrogen bond network in I  $\beta$  cellulose as  
730 observed by infrared spectrometry. *J Mol Struct* 523:183–196.  
731 [https://doi.org/10.1016/S0022-2860\(99\)00389-0](https://doi.org/10.1016/S0022-2860(99)00389-0)
- 732 Mariano M, El Kissi N, Dufresne A (2014) Cellulose nanocrystals and related  
733 nanocomposites: Review of some properties and challenges. *J Polym Sci Part*  
734 *B Polym Phys* 52:791–806. <https://doi.org/10.1002/polb.23490>
- 735 Mazeau K, Charlier L (2012) The molecular basis of the adsorption of xylans on  
736 cellulose surface. *Cellulose* 19:337–349. [https://doi.org/10.1007/s10570-011-](https://doi.org/10.1007/s10570-011-9643-7)  
737 [9643-7](https://doi.org/10.1007/s10570-011-9643-7)
- 738 Mihranyan A, Llagostera AP, Karmhag R, et al (2004) Moisture sorption by  
739 cellulose powders of varying crystallinity. *Int J Pharm* 269:433–442.  
740 <https://doi.org/10.1016/j.ijpharm.2003.09.030>
- 741 Nishino T, Matsuda I, Hirao K (2004) All-Cellulose Composite. *Macromolecules*  
742 37:7683–7687. <https://doi.org/10.1021/ma049300h>
- 743 Nishiyama Y, Langan P, Chanzy H (2002) Crystal structure and hydrogen-  
744 bonding system in cellulose I $\beta$  from synchrotron X-ray and neutron fiber  
745 diffraction. *J Am Chem Soc* 124:9074–9082.  
746 <https://doi.org/10.1021/ja0257319>
- 747 Nishiyama Y, Sugiyama J, Chanzy H, Langan P (2003) Crystal Structure and  
748 Hydrogen Bonding System in Cellulose I $\alpha$  from Synchrotron X-ray and  
749 Neutron Fiber Diffraction. *J Am Chem Soc* 125:14300–14306.  
750 <https://doi.org/10.1021/ja037055w>

- 751 Patera A, Derluyn H, Derome D, Carmeliet J (2016) Influence of sorption  
752 hysteresis on moisture transport in wood. *Wood Sci Technol* 50:259–283.  
753 <https://doi.org/10.1007/s00226-015-0786-9>
- 754 Patera A, Derome D, Griffa M, Carmeliet J (2013) Hysteresis in swelling and in  
755 sorption of wood tissue. *J Struct Biol* 182:226–234.  
756 <https://doi.org/10.1016/j.jsb.2013.03.003>
- 757 Qi H, Cai J, Zhang L, Kuga S (2009) Properties of Films Composed of Cellulose  
758 Nanowhiskers and a Cellulose Matrix Regenerated from Alkali/Urea  
759 Solution. *Biomacromolecules* 10:1597–1602.  
760 <https://doi.org/10.1021/bm9001975>
- 761 Rafieian F, Jonoobi M, Yu Q (2019) A novel nanocomposite membrane  
762 containing modified cellulose nanocrystals for copper ion removal and dye  
763 adsorption from water. *Cellulose* 26:3359–3373.  
764 <https://doi.org/10.1007/s10570-019-02320-4>
- 765 Safari S, van de Ven TGM (2016) Effect of Water Vapor Adsorption on Electrical  
766 Properties of Carbon Nanotube/Nanocrystalline Cellulose Composites. *ACS*  
767 *Appl Mater Interfaces* 8:9483–9489. <https://doi.org/10.1021/acsami.6b02374>
- 768 Salmén L (2004) Micromechanical understanding of the cell-wall structure. *C R*  
769 *Biol* 327:873–880. <https://doi.org/10.1016/j.crv.2004.03.010>
- 770 Sánchez-García MD, Hilliou L, Lagarón JM (2010) Morphology and Water  
771 Barrier Properties of Nanobiocomposites of  $\kappa/\iota$ -Hybrid Carrageenan and  
772 Cellulose Nanowhiskers. *J Agric Food Chem* 58:12847–12857.  
773 <https://doi.org/10.1021/jf102764e>
- 774 Sanchez-Garcia MD, Lagaron JM (2010) On the use of plant cellulose  
775 nanowhiskers to enhance the barrier properties of polylactic acid. *Cellulose*  
776 17:987–1004. <https://doi.org/10.1007/s10570-010-9430-x>
- 777 Sun H, Mumby SJ, Maple JR, Hagler AT (1994) An ab Initio CFF93 All-Atom  
778 Force Field for Polycarbonates. *J Am Chem Soc* 116:2978–2987.  
779 <https://doi.org/10.1021/ja00086a030>
- 780 Taylor DM (2002) Direct Cortical Control of 3D Neuroprosthetic Devices.  
781 *Science* (80- ) 296:1829–1832. <https://doi.org/10.1126/science.1070291>
- 782 Thommes M, Kaneko K, Neimark A V., et al (2015) Physisorption of gases, with  
783 special reference to the evaluation of surface area and pore size distribution  
784 (IUPAC Technical Report). *Pure Appl Chem* 87:1051–1069.  
785 <https://doi.org/10.1515/pac-2014-1117>
- 786 Wada M, Chanzy H, Nishiyama Y, Langan P (2004) Cellulose III I crystal  
787 structure and hydrogen bonding by synchrotron X-ray and neutron fiber  
788 diffraction. *Macromolecules* 37:8548–8555.  
789 <https://doi.org/10.1021/ma0485585>



- 790 Williamson RE, Burn JE, Hocart CH (2002) Towards the mechanism of cellulose  
791 synthesis. *Trends Plant Sci* 7:461–467. <https://doi.org/10.1016/S1360->  
792 [1385\(02\)02335-X](https://doi.org/10.1016/S1360-1385(02)02335-X)
- 793 Yu X, Tong S, Ge M, et al (2013) Adsorption of heavy metal ions from aqueous  
794 solution by carboxylated cellulose nanocrystals. *J Environ Sci* 25:933–943.  
795 [https://doi.org/10.1016/S1001-0742\(12\)60145-4](https://doi.org/10.1016/S1001-0742(12)60145-4)
- 796 Zhang C, Coasne B, Guyer R, et al (2020a) Moisture-induced crossover in the  
797 thermodynamic and mechanical response of hydrophilic biopolymer.  
798 *Cellulose* 27:89–99. <https://doi.org/10.1007/s10570-019-02808-z>
- 799 Zhang C, Shomali A, Guyer R, et al (2020b) Disentangling Heat and Moisture  
800 Effects on Biopolymer Mechanics. *Macromolecules* 53:1527–1535.  
801 <https://doi.org/10.1021/acs.macromol.9b01988>
- 802